GERDA

Progress report to the LNGS scientific committee

(Appendix)

LNGS-EXP 33/05 add. 7/08

The format of this GERDA progress report differs from our earlier ones to facilitate both fast and in-depth reading. A *short write-up* (`http://www.mpi-hd.mpg.de/GERDA/reportsLNGS/gerda-lngs-sc-oct08-shwup.pdf`) summarizes concisely the achievements during the last six months and highlights important issues. An *appendix* to the report (`http://www.mpi-hd.mpg.de/GERDA/reportsLNGS/gerda-lngs-sc-oct08-appdx.pdf`) provides additional technical and experimental details for follow-up reading.

October 2008

A.M. Bakalyarov [h], M. Balata [a], I. Barabanov [f], L. Baudis [m], C. Bauer [c], E. Bellotti [e], S. Belogurov [f,g], S. T. Belyaev [h], M. Barnabe-Heider [c], A. Bettini [j], L. Bezrukov [f], V. Brudanin [b], R. Brugnera [j], D. Budjas [c], A. Caldwell [i], C. Cattadori [a,e], O. Chkvorets [c], E. V. Demidova [g], A. Di Vacri [a], A. D'Androgora [a], V. Egorov [b], A. Ferella [m], F. Froborg [m], N. Fodyma [d], A. Garfagnini [j], A. Gangapshev [f], J. Gasparro [l], S. Gazzana [c], P. Grabmayr [k], G. Y. Grigoriev [h], K. N. Gusev [h], V. Gurentsov [f], W. Hampel [c], M. Heisel [c], G. Heusser [c], W. Hofmann [c], M. Hult [l], L.V. Inzhechik [h], L. Ioannucci [a], J. Janicsko [i], M. Jelen [i], J. Jochum [k], M. Junker [a], S. Katulina [b], J. Kiko [c], I.V. Kirpichnikov [g], A. Klimenko [b,f], M. Knapp [k], K.T. Knoepfle [c], O. Kochetov [b], V.N. Kornoukhov [f,g], K. Kroeninger [i], V. Kusminov [f], M. Laubenstein [a,e], V.I. Lebedev [h], D. Lenz [i], M. Lindner [c], J. Liu [i], X. Liu [i], B. Majorovits [i], G. Marissens [l], I. Nemchenok [b], L. Niedermeier [k], J. Oehm [c], L. Pandola [a], K. Pelczar [d], P. Peiffer [c], A. Pullia [e], F. Ritter [k], C. Rossi Alvarez [j], V. Sandukovsky [b], S. Schoenert [c], J. Schreiner [c], J. Schubert [i], U. Schwan [c], B. Schwingenheuer [c], M. Shirchenko [h], H. Simgen [c], N. Smale [c], A. Smolnikov [b,f], F. Stelzer [i], L. Stanco [j], A.V. Tikhomirov [h], U. Trunk [c], C.A. Ur [j], A.A. Vasenko [g], S.Vasiliev [b,f], M. Wojcik [d], E. Yanovich [f], J. Yurkowski [b], S.V. Zhukov [h], E. Zocca [e], G. Zuzel[c]

[a] INFN Laboratori Nazionali del Gran Sasso, Assergi, Italy
[b] Joint Institute for Nuclear Research, Dubna, Russia
[c] Max-Planck-Institut für Kernphysik, Heidelberg, Germany
[d] Institute of Physics, Jagellonian University, Cracow, Poland
[e] Università di Milano Bicocca e INFN Milano, Milano, Italy
[f] Institute for Nuclear Research of the Russian Academy of Sciences, Moscow, Russia
[g] Institute for Theoretical and Experimental Physics, Moscow, Russia
[h] Russian Research Center Kurchatov Institute, Moscow, Russia
[i] Max-Planck-Institut für Physik, München, Germany
[j] Dipartimento di Fisica dell'Università di Padova e INFN Padova, Padova, Italy
[k] Physikalisches Institut, Universität Tübingen, Germany
[l] Institute for Reference Materials and Measurements, Geel, Belgium
[m] Physik Institut der Universität Zürich, Zürich, Switzerland

Spokesperson: S. Schönert,
(Stefan.Schoenert@mpi-hd.mpg.de)
Co-Spokesperson: C. Cattadori
(Carla.Cattadori@lngs.infn.it)
Technical Coordinator: K.T. Knöpfle
(Karl-Tasso.Knoepfle@mpi-hd.mpg.de)

URL: http://www.mpi-hd.mpg.de/GERDA/reportsLNGS/

Contents

1 Cryogenic vessel and infrastructure

After the cryostat was delivered in March to LNGS, several acceptance tests have been performed. These are in chronological order

- a radon emanation measurement before the installation of the internal copper shield, which yielded an acceptable level of 13.7 ± 1.9 mBq of ^{222}Rn,[1]
- a helium leak test of inner and outer vessel which showed no leak at the 10^{-7} mbar·l/s range,
- an evaporation test with liquid nitrogen after the copper shield installation which gave a result consistent with the previous test at the production site (< 300 W heat loss), and
- another radon emanation measurement after the copper installation which yielded 34 ± 6 mBq.

The increase in emanation is most likely due to dust (10 grams of dust from Hall A emanate 24 ± 2 mBq) which entered into the cryostat during the copper plate mounting and - to a smaller extend - due to small, improperly cleaned, copper pieces. Hence a cleaning of the accessible surfaces on the inside by wiping with propanol wetted tissues is scheduled for the first week of November.

The results of the various tests at LNGS were rather gratifying: they showed not only that the cryostat performance did not deteriorate during the transport to LNGS but also that the entire procedure of filling and emptying the cryostat with liquid nitrogen worked very well.

The final documentation for the cryostat is currently checked by TÜV Nord and the formal certification of the cryostat is expected in November.

The cryogenic infrastructure was tendered beginning of the year. However, no acceptable offer was received. In the following negotiation process, the Dutch company DeMaCo was selected to build the infrastructure. As the first step the piping and instrumentation design was optimized, see Fig. 2. Main modifications to the previous design are:

- Triaxial lines with an inner process pipe for liquid argon, an outer process pipe for liquid nitrogen, and a vacuum jacket with multilayer insulation allow to subcool argon immediately after the extraction from the storage tank. A phase separator for argon as it was foreseen previously at level 9700 mm is therefore no longer needed and microphonic noise during argon refilling - if needed - should be minimal.
- A rupture disk in front of the safety valve for the cryostat allows maintenence of the valve without removing it and disturbing the measurement. Previously, the design

[1] A homogeneous distribution of 8 mBq would add 10^{-4} cts/(keV·kg·y) to the background index. If anti-coincidences between diodes and segments are applied for the phase II setup then the value increases to 14 mBq.

included two safety valves and a change-over valve which selected the second valve while the first one is removed for maintenence. The second advantage of this solution lies in the design of the rupture disks: it is fully metal sealed with a helium leak rate $< 10^{-8}$ mbar·l/s. Any radon emanation from the valve is therefore irrelevant. This is important since we found that cast stainless steel like it is used for the body of the safety valve and change-over valve emanates an unacceptable amount of radon.

All components of the system are identified and ordered. Components in contact with argon are metal sealed against atmosphere. Liquid argon is filtered by a large area PTFE filter with 50 nm pore size. Three level sensors will be installed: a swimmer by WEKA, a radar sensor by Krohne, and a pressure sensor which measures the pressure of an argon gas buffer which is in contact with liquid argon through a thin pipe. Inside the pipe, argon gas liquifies and hence the pressure decreases. The amount of liquification depends on the fill level, i.e. on the wetted area. This device is developed by DeMaCo.

Currently, the detailed design is in progress; as an example, Fig. 1 shows the layout of the valve box. Long lead items like the cryogenic valves are in production. The installation is expected for January 2009.

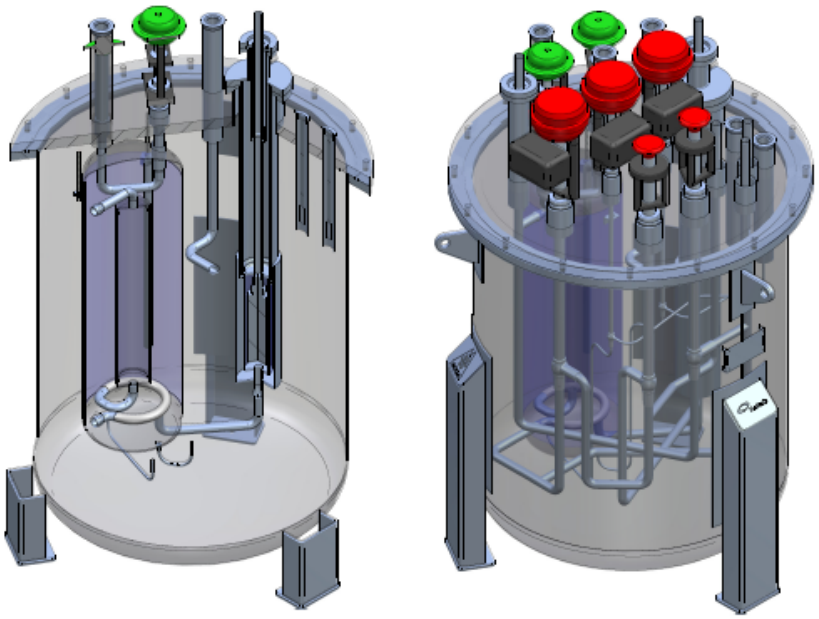

Figure 1: A total view of the valvebox (right), and a cut (left) showing more clearly the big LN cooled Rn trap (left) and the particle PTFE filter in the LAr line.

The heater for the exhaust gas has been ordered. It is an argon gas - water heat exchanger. The cooling water of LNGS (20 kg/s) will be used to heat 0.95 kg/s (2500 Nm^3/h) of cold gas to a temperature above 0 °C. If water with 12 °C and twice the through put is used even five times as much gas can be heated to about 0 °C.

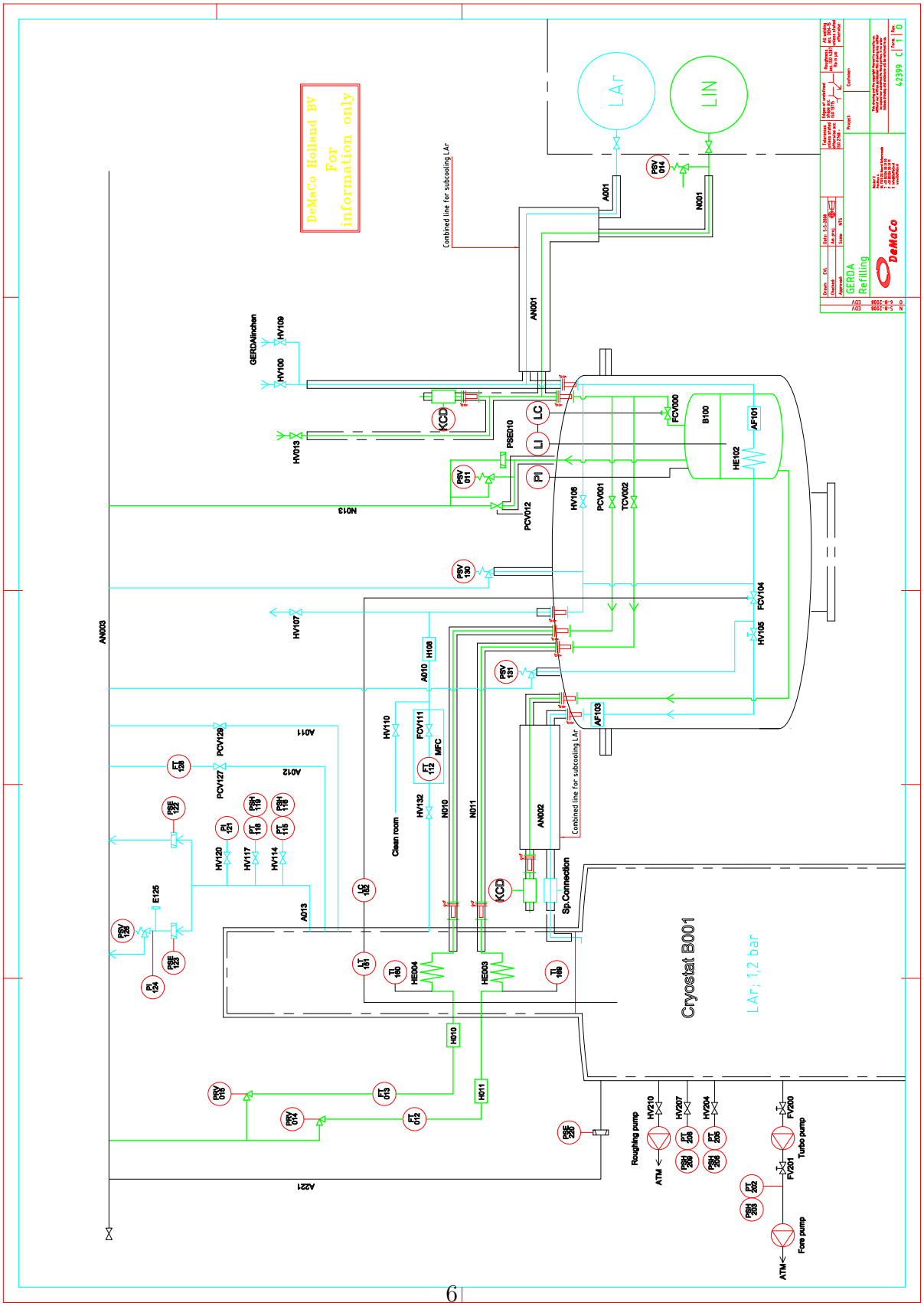

Figure 2: New Piping and Instrumentation Design from DeMaCo.

2 Status of Water Tank and auxiliary plants

The GERDA water tank (WT) construction in hall A of LNGS was completed in June 2008. Figure 3) displays two stages of the construction. The sequence of construction was carried out as described in our last report [1]. After completion, the following acceptance tests have been performed:

- Preliminary test of the bottom plate and water outlet flanges sealing: in June '08 the test has been performed filling the tank by approximately 80 m^3. No decrease of the water column height has been observed (within 0.5 cm accuracy) during the three days of the test. The water has been subsequently drained into the 3 x 100 m^3 pools located below the Hall A floor and removed by truck from underground.
- X-ray tests of 20 weld locations distributed on the lateral WT surface. The test has been performed on 26th July by a specialized company using an X-ray gun with 200 kV / 5 mA. All tested welds past this acceptance test.

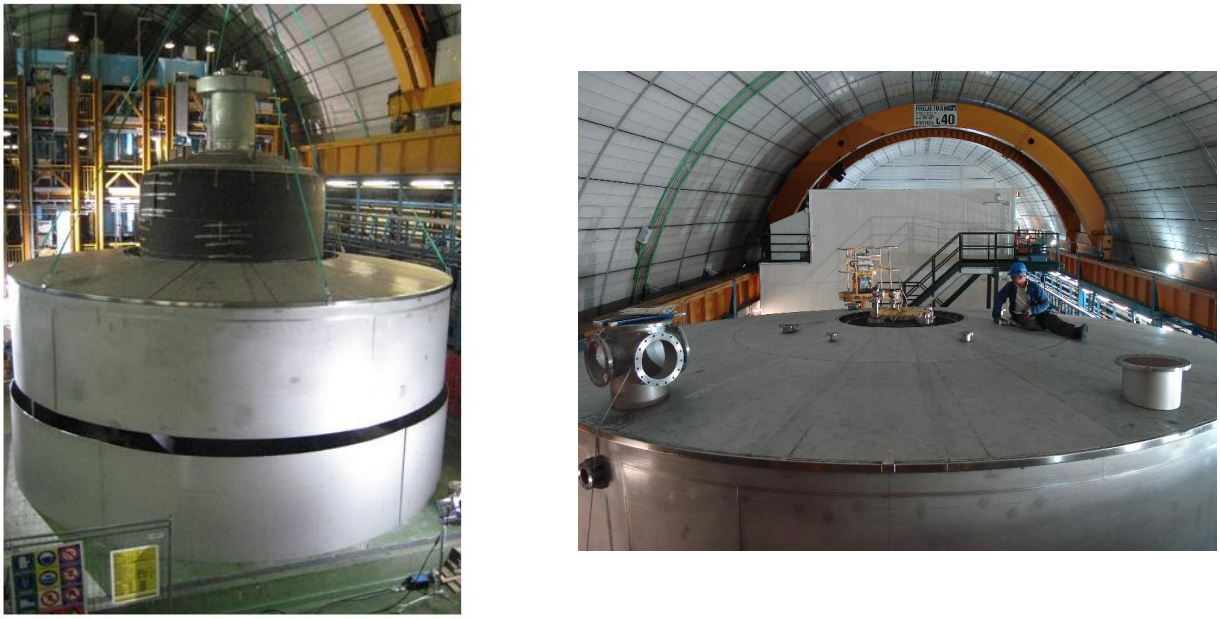

Figure 3: Two phases of the construction of the GERDA water tank on May- June 2008

Several other important tests and operations are currently in standby, because the authorization to drain water from the GERDA tank into the new water discharge network is not yet available. The request has been submitted by the LNGS to the Teramo authorities only on June 14, 2008. The pending works are

- the hydrostatic test of the tank,
- the steam cleaning of the inner tank walls,

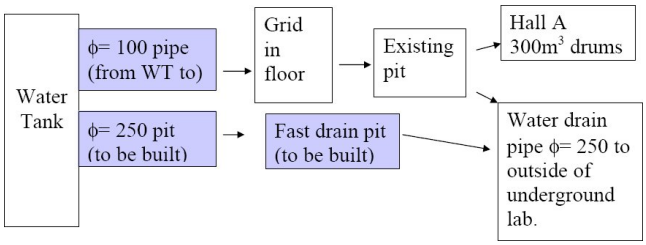

Figure 4: The schematic of the GERDA water drain: in blue the missing parts.

- and the mounting of the photomultiplier (PMT) and reflective foils for the water Cherenkov detector.

Other parts of the water system are well on their way: The line to connect the Borexino de-ionized water plant to the GERDA experimental site is under construction and the water plant to circulate and purify the water for Cherenkov light detection has been ordered. Delivery of the latter is projected for the end of 2008. Very recently, the INFN Commissione II has funded the GERDA-LNGS group to build the direct water drainage connection. Operating in parallel with the drainage into the 3 x 100 m^3 pools, this will allow to empty the complete the water tank within a couple of hours. This procedure was one important outcome of the GERDA risk analysis [2] for the case of a severe failure of the cryostat thermal insulation. The administrative procedure to tender the work has already started and the work will be completed by the end of 2008.

3 Progress of the construction work in hall A

The installation of the general infrastructure of GERDA in hall A is proceeding. Subsequent to the completion of the installation of the Water Vessel in June 2008 the construction of the GERDA building started. The structural work was completed beginning of October and a foto is displayed on the front page of this report . In the mean time, the wall panels of the building have been mounted. The contracts for implementing the safety plants and the electrical plants, incl. telephone, LAN and air conditioning are signed and the involved companies are preparing the installations.

The tube bringing the de-ionized water from the Borexino plant in Hall A to GERDA is under construction and the contract for the water recirculation plant of the water tank has been signed. These work will start in the immediate future.

The contract for the removal of the explosion prove door blocking the access for the storage area for liquid argon and liquid nitrogen has been signed. The authorization for the removal of the door was approved by the relevant authorities in October.

The tendering process for the construction of the water pit required to release the water to the drainage system of LNGS has been started.

Critical for the commissioning of GERDA is the timely completion of the design of the ventillation system and its installation by LNGS.

4 Clean room and lock system

4.1 The clean room

The final design of the clean room has been established. It will be a class 10.000 clean room with 30%±5% rel. humidity and a temperature of $21 \pm 2^0 C$. The volumes underneath the flow boxes will be of class 100.

For support of the clean room walls a steel frame will be built on top of the superstructure. This construction additionally allows for installation of a crane inside the clean room. The steel frame is designed to bear the muon veto on the clean room roof.

The tender has been closed. The company to build the clean room has been identified. They will receive the official order in CW44.

Construction will start CW03/09. The Clean Room is expected to be ready for use by CW12/09.

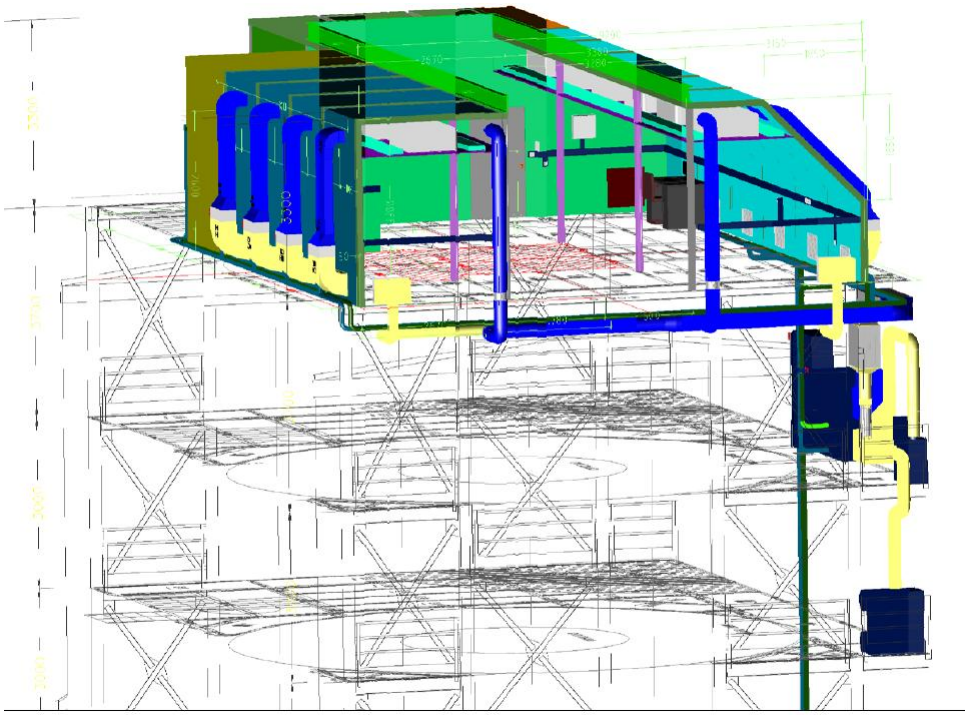

Figure 5: Design of the clean room on top of the GERDA tank. Note that the location of equipment on levels 6000mm and 3000mm will be exchanged.

4.2 Status of the commissioning lock

For the commissioning phase a simplified lock system allowing for insertion of strings with up to three detectors will be built. It consists of two linear pulleys that allow for lowering of two independent strings. The system is constructed such that one of the linear pulleys can be reconfigured to hold up to three strings.

The technical drawings of the system have been approved according to the pressure vessel code AD2000 in accordance with the cryostat.

All components of the commissioning lock system are available. The lock support structure has already been installed inside the dedicated clean room cabin at MPI für Physik in Munich. The installation of the lock cylinders will start CW45 and should be finished by the end of the year.

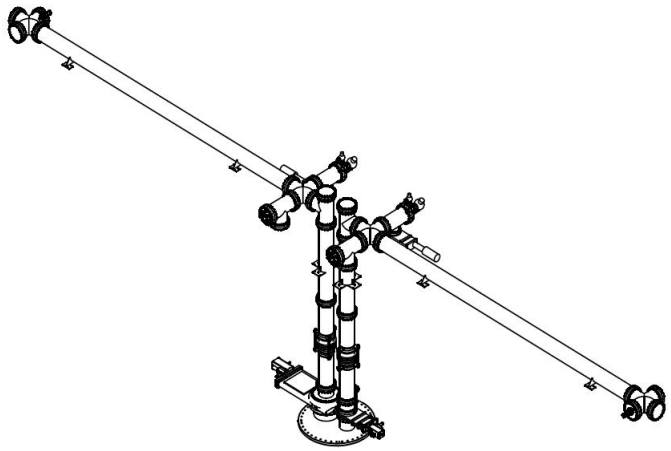

Figure 6: Drawing of the Commissioning Lock. The two linear pulley systems are housed inside the horizontal cylinders. The left vertical cylinders connected to the cryostat with a ISO250 shutter thus allowing for an increase of the cylinder diameter.

4.3 The final lock system

The mechanical design of the final lock system is being finished. The approval of the inner and outer lock cylinders according to pressure vessel code AD2000 and extraction of the construction drawings from the CAD model will be done by an external company.

The lock will be attached to a support structure that is bolted to the HEB700 beams of the GERDA superstructure. The support structure is resting on damping feet in order to decouple the lock system from high frequency vibrations. The design of the lock support structure is finished. The construction drawings will be finalized once the final alignment of the cryostat neck is known. This can only be measured once the cryostat and water tank are filled since the critical distances might change. With empty water tank and cryostat

the center of the cryostat neck is misaligned by 30mm on the N-S axis. The lock support design can be adjusted for a misalignment up to 50mm of the cryostat neck with respect to the HEB700 beams.

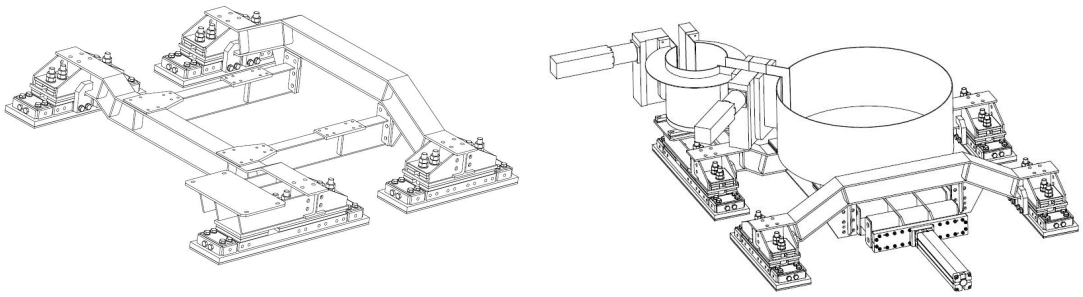

Figure 7: Drawings of the lock support with (right) and without (left) lock system attached to the structure.

The production of the linear pulley system components is ongoing and the assembly of the final lock system will start inside the aforementioned clean room (figure **??**) after completion of the commissioning lock system.

5 The Muon Veto

The GERDA muon veto has taken a major step towards completion. The production of the Cherenkov veto has been completed. In Fig. 8 a snapshot at the laboratory at Tübingen displays the production where 15 PMTs could be assembled simultaneously. This made it

Figure 8: Left: During the production of the encapsulations of the PMTs at Tübingen. Right top: The array of capsules during cleaning. Right bottom: The encapsulated PMT ready for testing an packing.

possible to finish 73 PMTs within 8 weeks. We will produce 8 more as spares, however are waiting for some components. The work was supported by members of the Double Chooz collaboration; in turn GERDA-members helped during the production of their ∼100 PMTs.

A complete PMT including the 32 m long cable is shown in Fig. 8, right bottom. At present each PMT is tested again and the results are compared to previous data. Parameters as dark current, gain and HV are stored in a data base for the running periods. Each detectors is wrapped and packed for transport to LNGS. The transport is foreseen for November 2008.

Procedures for mounting the PMTs have been developed. Two personal lifters are procured for safe operation of the mounting crew inside the water tank. The crew has had a safety training course at the company producing the personal lifter. Drivers licences have been issued. All necessary material has been procured. The final obstacle to start mounting is posed by the missing hydraulic test of the water tank due to the lack of authorization of the laboratory to drain the water after completion of the test. The LNGS directorate is in contact with the responsible local authorities, however it is unclear when the authorization will be available.

The second batch of plastic scintillators for the roof veto has been assembled. It is an improved version as the number of optical fibers has been doubled and better PMTs have

been employed. This batch will be delivered this fall to LNGS. Ongoing work concentrates on data acquisition and slow control.

6 Phase I detectors

The work during the last six months within task group one (TG-1) focused first on the completion of Phase I prototyping (work package three, WP3), and subsequently on the processing of the enriched and non-enriched detectors (WP4). Other activities concerned the construction and cryogenic tests of the low-background test stand LArGe (WP5). The main achievements during the last six months are

- the processing of all 17.9 kg of enriched and 15 kg of non-enriched phase I crystals at the manufacturer and their characterization in liquid argon with their final detector holder in the Underground Detector Laboratory Gdl at Lngs (WP4);
- the completion of the low-background LArGe cryostat, the successful testing of the active cooling system, the finalization of the cryogenic transfer lines, the preparation of the photomultiplier and wavelength shifting and reflector system (WP5).

6.1 Prototype testing

As summarized in the last report, we found that the gamma radiation induced leakage current increase was strongly reduced when covering only the groove area with the passivation layer. One of the three diodes under test was prepared without any passivation layer. We found that this treatment of the grove surface exhibited no gamma radiation induced leakage current increase even under long-term gamma irradiation.

To test the robustness of this detector technology, we carried out further warming and cooling cycles following our detector handling protocol. This includes exposure to nitrogen gas atmosphere during detector assembly mounting and handling, and warming up in alcohol. No deterioration of the detector performance was observed. Based on this experience, we decided to prepare all phase I detectors without covering the groove area with a passivation layer.

6.2 Diode processing and testing of Phase I detector assemblies

Prior to their operation in Gerda, the enriched and non-enriched phase I detectors have been operated in the LAr test facility of the Gerda underground detector laboratory (Gdl) at Lngs. The goal was to test each detector mounted in its low-mass holder and to measure its performance in LAr. After the reprocessing of the detectors, their operational parameters (depletion voltage, leakage current, resolution) have been measured and compared to the values measured in their vacuum cryostat. In total, eight enriched, two detectors from Genius T-F, and the Prototype no. 1 have been tested. The quality of the high voltage (HV) and signal contacts is measured after the mounting when the

Figure 9: Top: Radon reduced glove-box/clean bench with nitrogen atmosphere and integrated liquid argon cryostat for mounting and testing the final phase I detector assemblies. Bottom left: Removal of an enriched crystal from its vacuum transportation and storage container. Bottom right: Adjustment of the torque of the high-voltage contact.

detector is warm and remeasured after the cooling down of the detector assembly. The leakage current, the spectroscopy performance and the counting rate under the peak are measured in function of the applied bias high-voltage. The active mass of the detectors is determined relative to that of the prototype detector no. 1. Two of the enriched detectors have been processed already earlier with the application of the passivation layer over the full front-face area. The passivation layer of these two detectors are currently been modified at the manufacturer. Only one of the enriched detectors showed a leakage current which was higher than measured at the detector manufacturer. These three detectors have been processed again at the manufacturer in October and returned to Gran Sasso.

The activation by cosmic radiation has been minimized by point-to-point car transportation and underground storage. The exposure to cosmic rays above ground including transportation from LNGS to the manufacturer and back, and processing at the manufacturer, was typically less than five days. Thus the production of cosmogenic isotopes as ^{60}Co is negligible. The results are being summarized in the GERDA Scientific / Technical Report [3].

6.3 Low-background test stand LArGe

The construction of the vacuum insulated copper cryostat was completed successfully. Instead of standard super-insulating foils, a custom designed low-background PTFE/copper super-insulating sandwich layer has been mounted inside the vacuum spaces. The evaporation rate of the cryostat was determined. The heat load corresponds to an evaporation rate of 1.3 kg of nitrogen per hour or 70 Watt, meeting the design specifications of < 90 Watt. Subsequently, the cryostat was filled with liquid argon and the active cooling system tested. Liquid nitrogen at an overpressure of 1 barg is transfered into the heat-exchanger which is integrated into the neck of the cryostat where the transition to the gas phase occurs. The liquid nitrogen evaporates in the heat exchanger requiring 160 kJ/liter. The cooling power is controlled via a mass flow controller of the evaporated nitrogen gas at the outlet of the heat exchanger. The measured argon evaporation is less than 1 kg after 48 hours of continuous cooling at 1.8 kg liquid nitrogen per hour. This corresponds to a nitrogen gas flow of approximately 1.5 m^3 (STP) per hour. At a flow rate of 2 kg per hour, no mass loss was observed within two days. The mass loss is determined by measuring the weight of the cryostat with an accuracy of 1 kg. The temperature measurements showed that the liquid argon is sub cooled for nitrogen flows above 1.5 m^3. The design of the vacuum insulated transfer lines has been completed and the parts are tendered. The mass flow control units and temperature sensors are available and are under test.

The photomultiplier (PMT) system with its low-background voltage divider, designed for operation in the argon gas atmosphere, is in its assembly phase. The coating of the wavelength shifting reflector foil has been completed. Next steps are the integration of the PMT system into the cryostat followed by operational tests of the full system prior to its installation in the Gdl at Gran Sasso.

7 Phase II detectors

7.1 Prototype testing

The commissioning of our newly built test cryostat was finished in the spring, as we reported in the previous report. A new 18 fold segmented prototype was bought from Canberra France. For the first time ever we successfully operated an N type segmented HPGe detector in liquid nitrogen. From the insertion until the warm-up our detector operated for five month without measurable deterioration of the performance.

The measured leakage current was below $\sim$4 pA and was stable during the 5 months operating period. The detector was exposed to various radioactive sources, including ^{228}Th, ^{60}Co and ^{152}Eu. The core resolution of 4 keV (FWHM) at 1332 keV (^{60}Co line) was achieved. The resolution of the 18 segments varies between 4.5 and 7 keV, dominated by electronic and microphonic noise in the test stand. The detector performance was stable during the period of testing. As an example, Figure 10 shows the core energy spectra from the ^{228}Tl source for all events and for single-segment events only. Events in the double-escape peak (DEP) from the 2614.5 keV photon are expected to be mostly single-site events

and survive the single-segment cut, while events in the photon peak at 1620 keV are mostly multi-site events and are significantly suppressed by the cut.

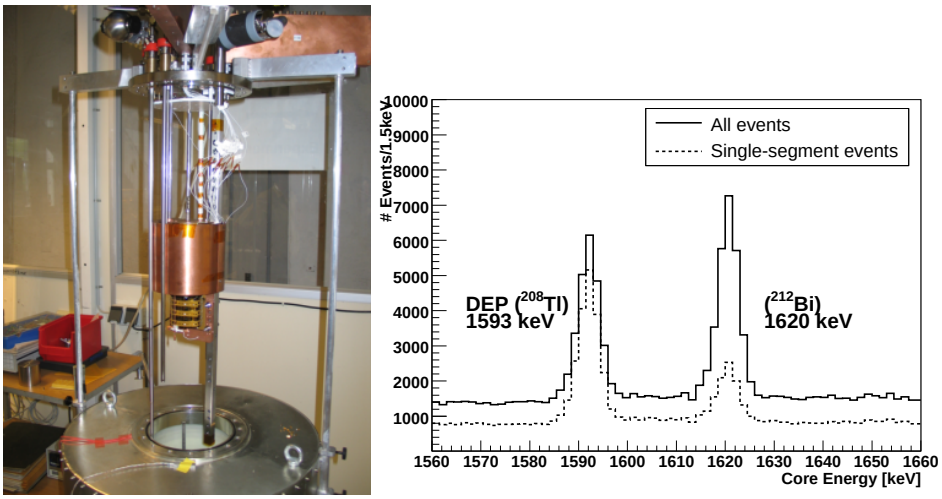

Figure 10: Left: the 18 fold segmented prototype is being lowered in the cryostat, Right: the measured core energy spectra with the detector exposed to a ^{228}Th source before (solid line) and after (dashed line) the single-segment cut. The core and segment energy threshold was set to 20 keV.

In parallel a 19 fold segmented prototype is being tested in vacuum inside a conventional cryostat. The 19th segment is 5mm thick circular segment on the top of our usual 18 segment configuration. It was designed to study the detector response close to the passivated surface.

7.2 Production of Phase II detectors

After a complete refurbishing the Czochralski puller set up at IKZ, Berlin was operated with success for the first time on April 7, this year. Already the second pulling attempt yielded a crystal with about 5 cm in diameter and a 10 cm cylindrical part (dimensions limited by the 4" crucible). Until now seven test crystals were produced so far. The starting material was standard 6N Germanium except for one crystal that was made of depleted Ge purified at PPM Pure Metals. The crystals were cut and samples were prepared for Hall-effect and Photo-Thermal Ionization Spectroscopy (PTIS) measurements.

7.3 Crystal characterization

The Hall-effect measurement and PTIS was done on three crystals grown so far and the analysis of the other crystals is on the way. Several samples were taken along the length of the crystals. The measurements showed an impurity level typically of $10^{13}/cm^3$. PTIS spectra are typically dominated by the phosphorus and arsenic lines (see Figure 11). Several

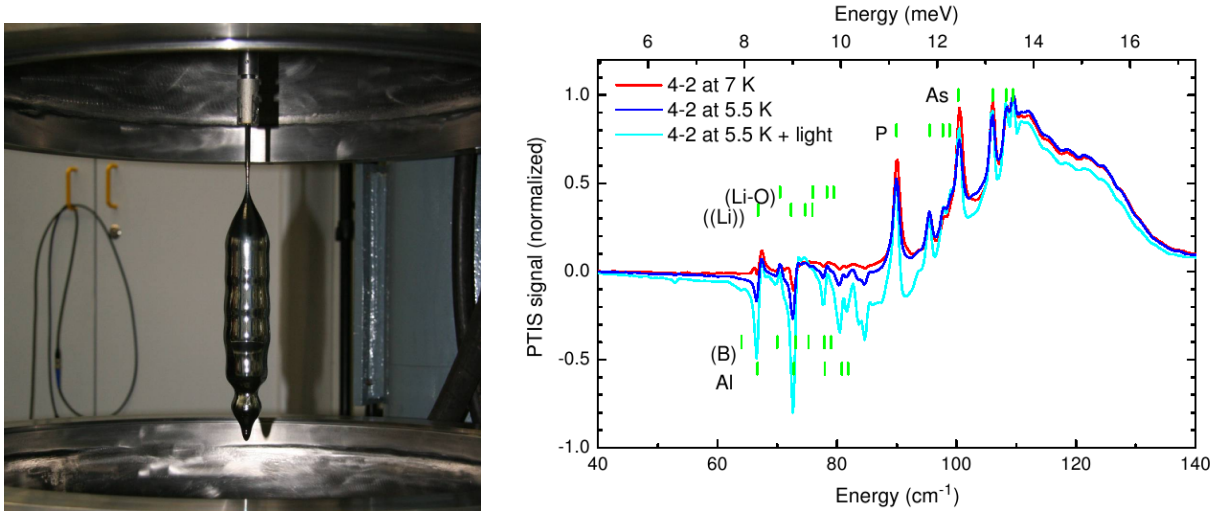

Figure 11: Left: Ge crystal just after the Czochralski puller was opened at IKZ, Berlin, Right: PTIS spectrum of the crystal grown at IKZ from material purified at PPM

measures are being taken to improve the purity of the crystals, like using Ultra High Purity crucibles and increasing the H_2 content of the forming gas.

The measurement methods used at IKZ were validated by an independent measurement at Berkeley and yielded similar numbers and the same PTIS spectra.

Quick turnaround on the crystal characterization is needed to keep up with the production rate of new crystals. To increase our analysis capacity the group from Dresden will join in these measurements. They are currently setting up their facilities with a reference crystal sample provided by IKZ.

7.4 Pulse shape studies with a p-type BEGe-detector

A new R&D on multi-site event (MSE) vs. single-site (SSE) event discrimination with an 81 mm x 32 mm (0.8 kg) modified BEGe p-type detector operated in a standard vacuum cryostat, has been carried out during the last six months at MPIK Heidelberg. This work was stimulated by refs. [4, 5]. Measurements with different sources were carried out to characterize the detector response and efficiency, and to determine quantitatively the signal-like/background-like event discrimination power. The energy resolution was 0.49 keV (FWHM) at 59 keV and 1.6 keV (FWHM) at 1332 keV. The homogeneity and isotropy of the detector response was verified by scanning the crystal with a collimated ^{241}Am source.

The 1593 keV double escape peak (DEP) from the 2614 keV ^{228}Th line contains dominantly single-site events, similar to neutrinoless double beta decays, while the typical background lines are mostly multi-site. Adjusting the acceptance of the recorded DEP at 91%, the Compton continuum in $Q_{\beta\beta}$ region is reduced to 49% in the ^{228}Th spectra, to 31% in the ^{226}Ra spectra and to 1.6% in the ^{60}Co spectra. The MSE rejection was tested

with the single escape peak (SEP) from the 2614 keV ^{228}Th line, which is suppressed to 9% of its initial intensity, and with the 2505 keV summation peak of ^{60}Co gamma lines, suppressed to 0.5%. Both the SEP and the summation peak contain dominantly MSE. Figure 12 displays part of the ^{228}Th spectra with the DEP and the 1620 keV full energy (FE) peak. The FE peak containing mostly MSE is suppressed to 13% of its initial intensity. Refinements of the analysis and additional measurements using two germanium detectors for single Compton scattering to produce SSE events with energies at $Q_{\beta\beta}$ are ongoing.

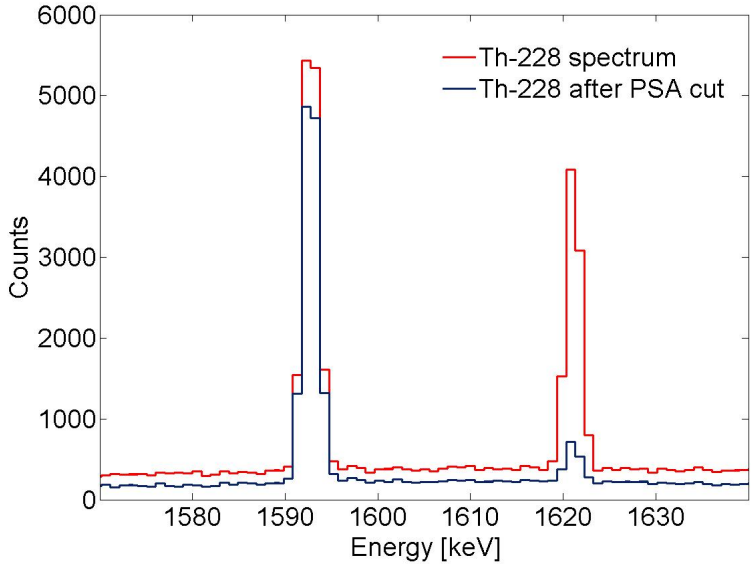

Figure 12: Pulse shape discrimination studies with a BEGe-type detector. The red spectra corresponds to all all events, while the blue spectra is obtained after applying the pulse shape analysis (PSA) cut. Here, the acceptance of the DEP has been adjusted to 91%, which leads to a suppression of the multi-site dominated 1620 keV line of 13% of its initial intensity. The Compton continuum is reduced to 49%.

8 Front end electronics

8.1 Status of PZ0 for phase I

In April 2008, the final front end (FE) circuit has been selected: it is a CMOS ASIC with discrete input J-FET and feed back components, named PZ0. Connected to the SUB encapsulated p-type detector it yielded an energy resolution of 2.3 keV with a ^{60}Co source. Extensive tests with a bare prototype detector have been performed in the test bench 2 of the GDL laboratory during the summer months; thereby the ASIC was mounted with a

ceramic carrier onto a PCB. The results are reported in the following subsection. Moreover, these tests allowed to identify improvements which have been implemented in the final 3-channel PCBs that will allow to operate the 3-channel version of the PZ0, 25 dies of which are available since the beginning of 2008. These chips will be used for the readout of the phase I detector strings one being mounted on top of each string. The design of the 3-channel PCBs started in September 2008 and is now complete. In order to minimize radioactivity, the PCBs will be made from Cuflon, SMD 0402 components will be used, and the chips will be bonded as die directly onto the substrate. The circuit bench test is planned for the end of November; it will be followed by tests with the SUB encapsulated detector as well as with bare detectors mounted in a string.

8.2 Results of PZ0 coupled to phase I prototype

From June to August 2008, extensive tests of the PZ0 circuit connected to the bare prototype detector were performed with the following scopes and results:

- *Measurement of the energy resolution obtainable with the PZ0 ASIC, the bare prototype detector operated in LAr, and realistic mount and cabling.*
  Connected to the protoype detector the energy resolution obtained so far is 3.2 keV for the 1332 keV gamma line of ^{60}Co. If the detector is replaced by a capacitor of C_{det}= 33 pF, a resolution of 1.4 keV is measured.
  From a background spectrum accumulated during 12 hours, the full width at half maximum (FWHM) of the observed lines has been determined between 300 keV and 1.8 MeV (see Fig. 13). Comparing the ordinate intercept of about 3 keV with that found in the measurement with the capacitor, it is clear that an extra noise source is present when the PZ0 is connected to the detector. This extra noise cannot be attributed to the leakage current which was about 40 pA, and it has been shown to be not due to noise introduced by the high voltage bias voltage. The FFT of the baseline waveforms (see Fig. 14) indicates that the excess noise has a strong 1/f contribution, and additional data at lower frequency are needed to quantify this statement. The origin of the excess noise remains still to be identified.

- *Search for eventual problems related to the PCB, contacts and the grounding scheme.*
  Several improvements have been found and implemented in the 3-channel PCBs.

- *Test of different connection schemes of HV filter and FE circuits at the end of the cables string.*

- *Test of the full pulse processing and DAQ chain from detector to data storage.*
  The full DAQ chain has been used to collect and store pulses, and it behaved well. Fig. 15 shows a pulse collected when irradiating the detector with a ^{60}Co source. The JspecView suite has been adopted to perform the DAQ, the event display, the FFT analysis and the accumulation of the energy spectra. The energy resolution of the spectra derived from waveform analysis is poorer at present (3.6 keV) than the

one obtained by processing the pulse through the spectroscopy chain. This could be related to the fact that the analog signal of the PZ0 had to be splitted in order to create the trigger pulse; this is no longer needed.

- *Test the 1-channel sealed HV feed-through produced with the modified technology.* The origin of the noise related to the HV line has been identified and eliminated. The FWHM of the pulser line, corresponding to 1.4 MeV energy deposition, with C_{det}=100 pF, HV = 3 kV is found to be 2.6 keV at 3 μs shaping time. The HV sealed flanges and cables have a dissipation current that is less than the detector reverse current.

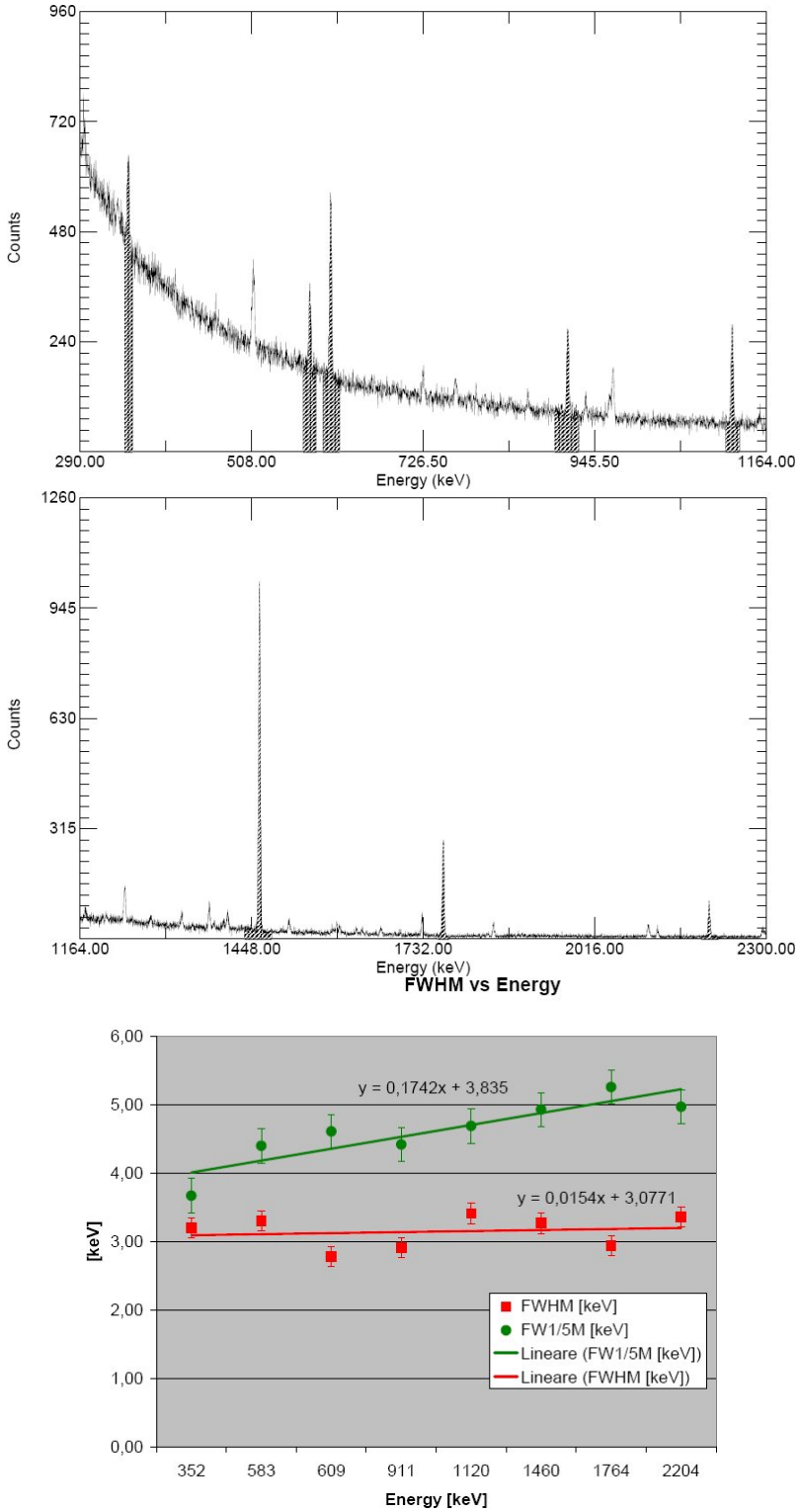

Figure 13: The background energy spectrum as measured with the PZ0 ASIC connected to the prototype detector (top), and the widths (FWHM and FW1/5M) of the marked gamma lines as a function of their energy (bottom).

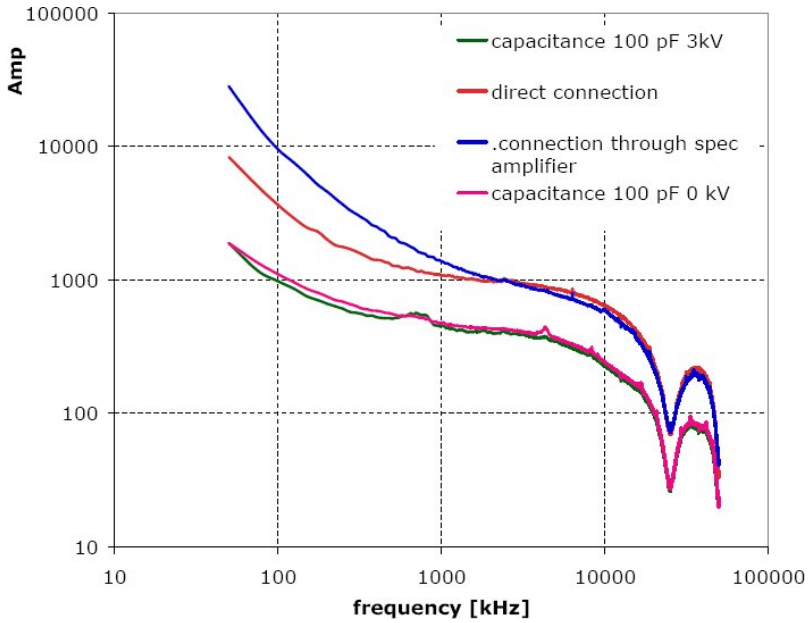

Figure 14: The modulus of the amplitude of the FFT in arbitrary units as a function of frequency as obtained from baseline waveforms. The waveforms have been collected with the digitizer that will be used in GERDA Phase I.

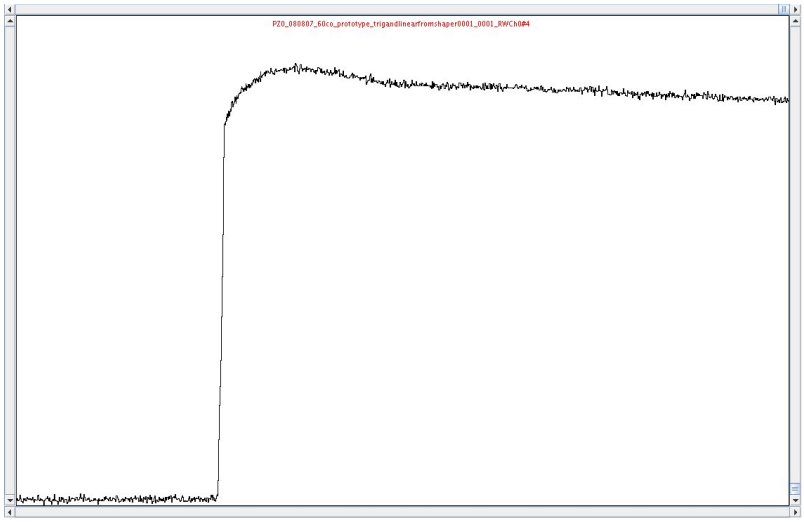

Figure 15: Waveform of a 1.332 MeV event in the prototype detector collected with the PZ0 charge sensitive preamplifier and digitized with the system that will be used in GERDA phase I. The waveform is reconstructed from 4096 digitizations at 100 MHz covering thus about 40 μs.

9 DAQ electronics and online software

The work on the PCI based digital data acquisition system focused on the following main tasks: improving the data throughput, synchronization of the data provided by different acquisition cards and implementation of a digital trigger algorithm.

While the normal data taking will not require the transfer of large volumes of data given the low event rate, during the calibration with standard γ-ray sources the system has to perform at high counting rates to minimize the period of time for exposing the Ge detectors to the gamma radiation. For this reason we developed a DMA based readout mechanism for the PCI cards that ensures an increase of the data throughput by a factor almost 10 as compared to the interrupt-based readout procedure. Tests with several cards have revealed some instability in the operation with the DMA procedure. We had to rework the VHDL code implemented in the Altera FPGA's and with the latest release of the Altera development software we fixed the malfunctioning of the system.

The implementation of the DMA data transfer protocol has, however, raised a new problem connected with the synchronization of the data read from the several PCI boards. We developed at the level of the FPGA a mechanism through which only one card is allowed to send out the interrupt request only after all the cards has finished the DMA data transfer from the PCI boards to the RAM memory. This mechanism produced only a very slight effect on the data throughput. Work is now in progress to adjust the data acquisition programs to deal with the new way of operation of the PCI cards.

Another important issue was finding a way to eliminate the necessity of splitting the preamplifier signals for producing the trigger signal needed for starting the readout of the data from the PCI boards. This problem was solved by implementing a simple trigger algorithm in the XILINX FPGAs mounted on the NIM boards. The work was done by INFN Padova and Milano. The algorithm based on a dual delay line procedure allows for very good performances as concerns the low threshold values and the elimination of the jitter of the trigger due to the time walk of the Ge signals. The algorithm was tested with a GASP Ge detector and standard γ-ray calibration sources at the National Laboratories of Legnaro. The value of the thresholds can be individually programed for each channel from any PC through a parallel port. The trigger signals from each channel are send to a multiple connector mounted on the back side of the NIM modules as TTL signals and they can be used to produce the general trigger signal of the Ge detectors system. A prototype card is ready and under tests. As soon as the tests are considered conclusive all the cards will be modified at the electronic workshop of INFN Padova.

The general plan of the slow control was defined during the first months of the year and its layout was illustrated in the last GERDA progress report. The activity of the Padova group is now focused on the realization of the slow control. The first hardware in the process of being controlled and monitored are the VME crates of the muon veto system and the NIM crates of the FE electronics and of the DAQ system. The software developed consists of a client program for talking with the crates through CAN bus, a PostgreSQL database

for data storage, an alarm system based on the ETRAX 100 LX Multi Chip Module [2] (for details see [6]) and a WEB browser for user interface. The CAEN HV SY1527LC power supply for the muon veto system will be the next hardware to be integrated.

In parallel to the slow control activities, some preliminary studies have been performed on the network structure for the GERDA building in Hall A. The plan is to create a local network among the computers in the GERDA building and a reliable connection with the external world. Padova group will profit from the expertise of the Padova INFN Computing Center.

10 Simulations and background studies

10.1 Simulation of the GERDA background spectrum

The activity of the Task Group 10, which is devoted to Monte Carlo simulations and background studies, was focused in the last six months on the preparation and start-up of a new major simulation campaign for GERDA (MCC2). The goal of the MCC2 campaign is to produce a realistic background spectrum for GERDA (also in the energy region below $Q_{\beta\beta}$), taking into account the most recent information about set-up geometry and material radiopurity. The Monte Carlo framework MAGE [7] has been updated and upgraded in order to meet all requirements for the MCC2 (geometry, primary generators, additional tools).
Two configurations of the detector array are taken into account in MCC2, labeled as "Phase I" and "Phase II". The detector array in the "Phase I" configuration includes 14 detectors: eight enriched non-segmented detectors (existing detectors from IGEX and Heidelberg-Moscow) and six non-enriched non-segmented detectors (existing crystals from GTF, Genius Test Facility). The detector array for "Phase II" contains 28 detectors: 14 non-segmented detectors from "Phase I" (IGEX, Heidelberg-Moscow and GTF) and 14 new enriched segmented detectors (18-fold segmentation, as in the prototype operated at the MPI-Munich). All existing detectors are modeled in MAGE with the real dimensions and weights. The model includes individual holders, cabling for electronics and support strings.

As a preliminary step, a set of simplified Monte Carlo simulations was performed to optimize the arrangement of the detectors in the available positions of the "Phase II" array. In particular, the relative horizontal distance between the detector strings has been varied in the two arrangements sketched in Fig. 16. A tighter scheme (e.g. a more compact array) improves the background identification by anti-coincidence but decreases the effective Liquid Argon (LAr) shielding between the strings, and vice versa. The background sources considered for the preliminary estimate are ^{60}Co and ^{68}Ge in the germanium crystals and the 2.6-MeV γ-rays from ^{208}Tl decays in the crystal holders and contact cables. For the "Phase II" configuration, the "horizontally-tight" array scheme (left in Fig. 16) results in a total energy spectrum (with segment anti-coincidence) which is 10% lower than the

[2] produced by AXIS Communications AB

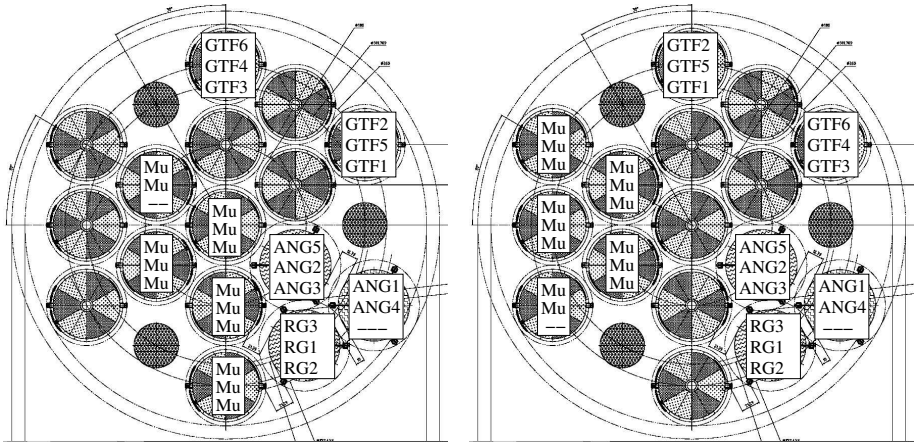

Figure 16: Schematic top-view onto the GERDA "Phase II" detector array. The names in the boxes indicate the detector type used in the first, second and third row of each detector string. The left figure shows the "horizontally-tight" scheme and the right figure the "horizontally-separated" scheme.

"horizontally-separated" array scheme.

The "horizontally-tight" array scheme is therefore considered as reference design for the MCC2 campaign. All relevant background sources are taken into account: internal contaminations, γ-rays from the environment and from the GERDA materials, cosmic ray muons (and secondaries), neutrons from radioactivity. The background rejection achievable with the detector and segment anti-coincidence is evaluated for each individual source. Only energy depositions in enriched detectors are considered, while GTF detectors are used for anti-coincidence. The core and segment energy threshold is 10 keV.
The neutrinoless $\beta\beta$-decay signal has been simulated with MAGE in order to evaluate the signal identification efficiency. Neutrinoless $\beta\beta$-decay events have been generated with the DECAY0 code [8], in the assumption that the process is mediated by a massive Majorana neutrino. In particular, the probability that a genuine neutrinoless $\beta\beta$-decay in one of the enriched detectors in the "Phase II" array produces an energy deposit in a 10-keV window at $Q_{\beta\beta}$ is: (92.0±0.1)% without any cut, (91.3±0.1)% with detector anti-coincidence and (87.2±0.1)% with segment anti-coincidence (statistical uncertainties from Monte Carlo).
In Fig. 17 are displayed the energy spectra for neutrinoless $\beta\beta$ events produced in the active volume and in the dead layer of the enriched crystals. In order to evaluate the expected signal in GERDA in the assumption of the neutrinoless $\beta\beta$-decay claim by Klapdor-Kleingrothaus *et al.* [9], the spectra are normalized for $T^{0\nu}_{1/2} = 1.2 \cdot 10^{25}$ y.

Background from cosmic-ray muons and from environmental neutrons has been estimated with MAGE-based simulations in the framework of MCC2. Results for the prompt muon-induced background are qualitatively similar to those published in Ref. [10], which

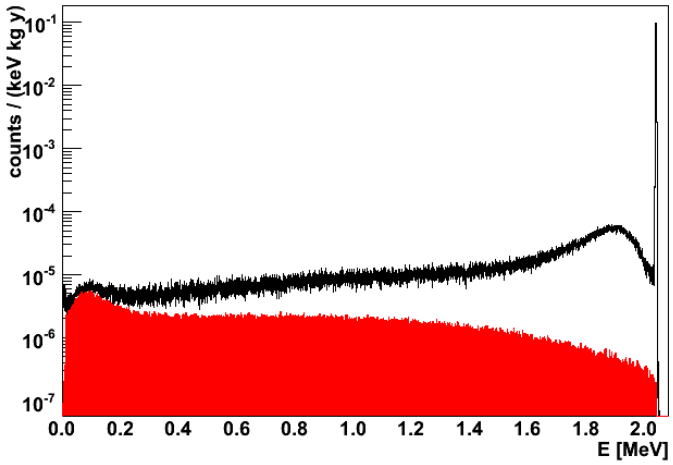

Figure 17: Sum of the energy spectra of the "Phase II" enriched detectors due to neutrinoless $\beta\beta$-decay of ^{76}Ge, in the assumption of half-life $T^{0\nu}_{1/2} = 1.2 \cdot 10^{25}$ y reported by Klapdor-Kleingrothaus *et al.* [9]. The black and red histograms show the spectra for events produced in the active volume and in the dead layer of the ^{enr}Ge detectors, respectively. Segment anti-coincidence has been required. The thickness assumed for the dead layer of p-type crystals in GERDA is 0.8 mm. Dead layer is considered to be negligible for n-type detectors.

had been derived with a different GERDA geometry and detector array. Fig. 18 displays the energy spectrum for the "Phase II" array from prompt muon-induced interactions. The background index at $Q_{\beta\beta}$ is $8.8{\cdot}10^{-3}$ cts/(keV·kg·y) (no cut), $5.4{\cdot}10^{-4}$ cts/(keV·kg·y) (detector anti-coincidence) and $3.7{\cdot}10^{-4}$ cts/(keV·kg·y) (segment anti-coincidence). As already discussed in Ref. [10], detector anti-coincidence is very effective for background rejection because muons produce large showers; the average multiplicity for events at 2 MeV is about 4 detectors and 6 segments. When the Cherenkov muon veto is taken into account, the count rate due to muon-induced background is reduced below 10^{-5} cts/(keV·kg·y) [10]. Dedicated Monte Carlo simulations to evaluate the efficiency profile of the Cherenkov veto vs. energy are presently ongoing, but an average efficiency $> 99\%$ is anticipated.
The muon-induced delayed background, namely the background due to long-lived unstable isotopes produced by muon-initiated cascades (e.g. ^{77m}Ge in the detectors, ^{41}Ar in the LAr buffer, etc.) will be evaluated by dedicated MAGE-based simulations within MCC2.

Similarly, the GERDA background due to low-energy neutrons (< 10 MeV) produced by natural radioactivity has been evaluated within the MCC2. Since the neutron flux coming from the LNGS rock is effectively suppressed by the thick water buffer, the main contribution comes from neutrons produced inside the GERDA geometry, specifically the stainless-steel cryostat. The neutron production rate from the cryostat, due to ^{238}U spontaneous fission and (α,n) reactions, is estimated to be $1.86 \cdot 10^3$ n/(ton·y), with average

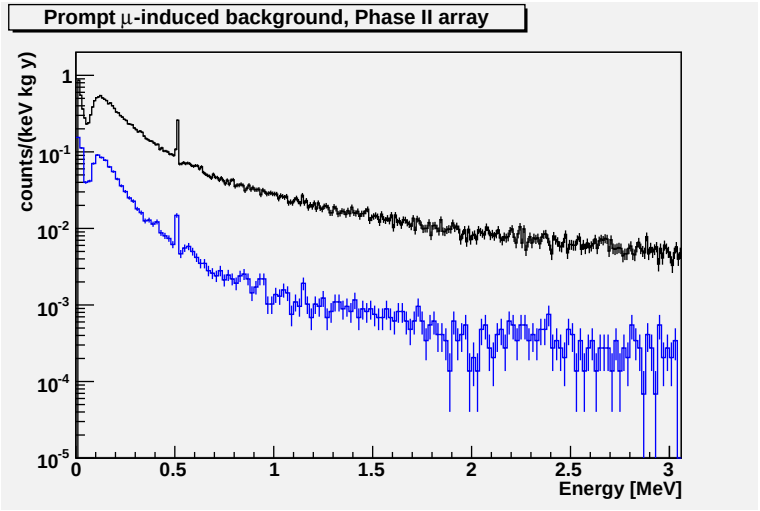

Figure 18: Sum of the energy spectra of the "Phase II" enriched detectors due to μ-induced interactions (prompt component only) up to 3 MeV. The black histogram shows the sum energy spectrum without any cut; the blue histogram shows the background suppression that can be achieved by segment anti-coincidence in the detector array. The only visible γ-line above the continuum background is the 511-keV annihilation peak.

energy $\langle E \rangle = 1.62$ MeV. The prompt background in the "Phase II" array induced by low-energy neutrons from the stainless steel, mainly via (n,n'γ) and (n,γ) interactions, is about $7 \cdot 10^{-6}$ cts/(keV·kg·y) (no cuts). Detector and segment anti-coincidence suppress the background by a factor of two and four, respectively. This is the first complete estimate of neutron-induced background in GERDA.

10.2 Simulation of pulse shapes from Ge detectors

During the last six months, relevant progresses have been made toward a full realistic simulation of pulse shapes from germanium detectors. The final goal is to provide a full-chain simulation of the data that will be available in GERDA, to be used to tune and benchmark the reconstruction and data analysis algorithms.
The important ingredients to be taken into account for a full pulse shape simulation are: (1) simulation of energy deposition in the detectors (done with MAGE); (2) calculation of the electric and weighting fields; (3) drift of the charge carriers through the crystal; and (4) model of the preamplifier and DAQ properties.
Numerical calculations of the electric field profiles and of the weighting potentials in the n-type true-coaxial detectors foreseen for "Phase II" have been completed. The model used for the electric field calculation takes into account the impurity density in the crystals. The agreement between numerical calculations and the analytical solution of the field equations is better than 0.6%. Similarly, calculations of the drift velocity of the charge carriers inside

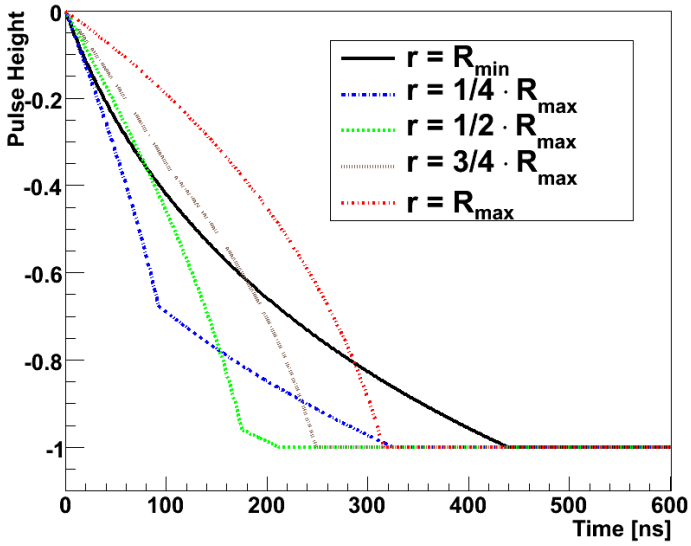

Figure 19: Simulated raw pulse shapes from the core of a n-type true-coaxial germanium crystal for a point-like energy deposition. The energy was deposited at different radial positions, in the range between the inner radius (R_{min} = 5 mm) and the outer radius (R_{max} = 37.5 mm) of the detector. No noise, preamplifier or DAQ properties are taken into account.

the crystals have been completed, taking into account the influence of crystal axes. Simulated pulses for unit energy deposition in the crystal core and in the segments have been produced accordingly. Fig. 19 shows the calculated pulses for different starting positions along the radial coordinate. It can be observed how the total length of the pulse and the time of the kinks in the pulse depend on the spatial position of the energy deposition. The final step to achieve a realistic pulse shape simulation is to convolve the ideal pulses of Fig. 19 with the response function of the electronic chain, including noise, bandwidth, etc. Following this step, simulations will be compared to real pulses acquired with the GERDA prototype crystals.

10.3 Investigation of LAr scintillation light and optical properties

The response function and optical properties of LAr scintillation have been investigated in a dedicated test facility called MiniLArGe [11]. The detector (19 liters of active volume viewed by one PMT) has been irradiated with a mono-energetic ^{148}Gd α source of energy 3.18 MeV.
Monte Carlo simulations based on MAGE have been compared to experimental spectra for different source positions. Monte Carlo simulations have been used to tune several unknown

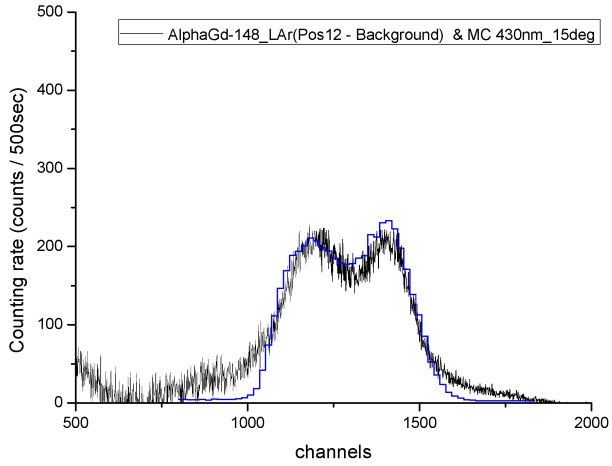

Figure 20: Amplitude spectrum from LAr irradiated with a mono-energetic ^{148}Gd α source. Experimental data (black histogram) are super-imposed with the corresponding MaGe-based Monte Carlo simulation (blue histogram).

optical properties of the set-up, as for instance the thickness of the TPB wavelength-shifter, the exact geometry of the ^{148}Gd source and of the VM2000 reflector foils, etc. A reasonable quantitative agreement between expected and measured spectra has been obtained for all source positions taken into account (see for instance Fig. 20).

11 Material screening

11.1 Radon emanation measurements

11.1.1 ^{222}Rn emanation measurements of the GERDA cryostat

The ^{222}Rn emanation of the GERDA cryostat (with pickled inner surface) was already investigated twice before the internal copper shield was installed: At the SIMIC company site and after the transportation to the Gran Sasso laboratory. The measured emanation rate was approximately 14 mBq (in saturation) which is low compared to cryogenic vessels of similar size measured in the past and acceptable for the experiment (corresponding background index of $2 \cdot 10^{-4}$ cts/(kg·keV·y) with no cuts and homogeneous ^{222}Rn distribution in the liquid argon). For the measurements the cryostat was closed with a steel flange sealed with a Helicoflex gasket and evacuated/filled with radon-free nitrogen twice (removing air-born ^{222}Rn). The third filling was done up to 1.6 barg and this gas was used later during extractions as a carrier gas.

After the copper mounting the emanation test was repeated. However, due to limited

time for preparation the vessel was evacuated only once down to 1.4 mbar before filling to overpressure. Two subsequent extractions were carried out two weeks later giving an average emanation rate of (121 ± 4) mBq. Two explanations of the measured excess of ^{222}Rn compared to the previous test were possible: Contaminations introduced by the copper mounting or residual air-born ^{222}Rn left over due to insufficient pumping. In order to investigate the first hypothesis a series of measurements on small components which were introduced along with the copper shield was performed (see subsection 11.1.2). No sufficiently strong source could be identified, therefore it was decided to repeat the emanation measurement of the cryostat 6 weeks after the first one. If there was air-born ^{222}Rn remained in the cryostat during the first measurement it has decayed completely since then. As always two extractions have been performed yielding an average emanation rate of (34.4 ± 6.0) mBq clearly confirming the hypothesis of residual air-born ^{222}Rn in the cryostat during the first test.

However, the cryostats emanation rate is still somewhat above the acceptable value. Therefore, an additional cleaning of the cryostat with subsequent emanation test is still necessary.

11.1.2 Emanation measurements of small components

The investigation of samples by means of the ^{222}Rn emanation technique was continued also in the current reporting periode. Besides materials foreseen to be used in the GERDA lock a campaign was performed to identify possible sources of contamination of the cryostat. Further samples were gloves, tubes, cables and a piece of diamond abrasive paper. The results are summarized in Table 1. In the first box samples for the lock are shown. All emanation rates lie between few and few tens of μBq for individual pieces which is usually acceptable. The only exception are the SIMRIT o-rings: Here we are seeking for an alternative, because many of them will be used posing stronger limits on the individual pieces.

After the discovery of the increased ^{222}Rn emanation rate of the cryostat after the copper mounting possible sources were investigated. All candidates which went into the cryostat along with the copper were screened: Silvered screws and paintings with a black permanent marker showed no measurable emanation rate. The copper bolts may explain part of the excess whereas the remaining fraction is probably due to dust contaminations during mountig or due to contaminations on the copper surface itself. Therefore, a final cleaning of the cryostat by alcohol wiping is envisaged. Lint-free wipes showed a non-negligible ^{222}Rn-emanation rate, however, no ^{226}Ra should be released by them.

We have investigated several flexible tubes: For different types of stainless steel tubes we found emanation rates between ~ 5 μBq/m and ~ 30 μBq/m including different kinds of flanges. These tubes will be used inside the cryostat and in the cryogenic infrastructure. For a polyamide tube we found only an upper limit of < 7.1 μBq/m.

Interesting result were obtained for gloves: Nitrile gloves showed a strong ^{222}Rn emanation rate. This holds not only for long-sleeve multiple use gloves, but even for single-serving gloves which have a much smaller mass. Therefore, normalized to the mass, nitrile emanates

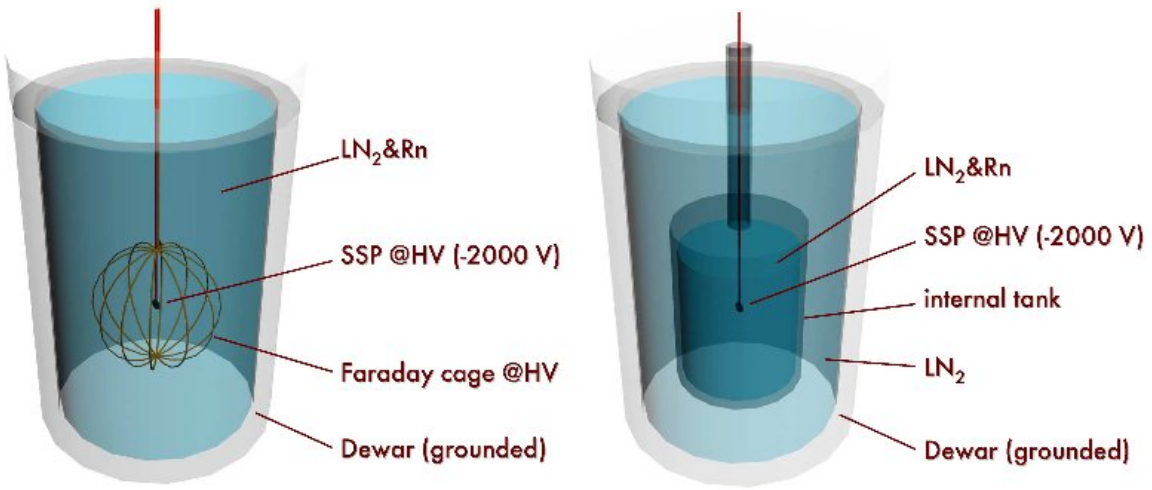

Figure 21: The two experimental setups used to study the behaviour of radon in liquid nitrogen. See text for further explanations.

even more ^{222}Rn than viton which is already known to be a substantial ^{222}Rn emitter.

11.2 Radon monitoring

The electrostatic radon monitor mentioned in the last progress report works well with a high voltage of up to 35 kV for radon in nitrogen. For the first time, we proved the ability to measure within gaseous argon. With respect to the argon the monitor works well up to 12 kV without discharges. Using a larger silicon PIN detector and electrostatic focussing, the collection efficiency was determined to be 20 % and could be improved to 95 % for nitrogen using 35 kV and for argon using 10 kV. Furthermore, a two month long-term measurement was carried out successfully with low radon activity.

An aqueous $RaCl_2$ solution of known activity was used to provide a homogeneous radon concentration inside the detection system for calibration. Also the background of the radon monitor was investigated: Within 6 days an increase of the radon concentration by a few mBq/m^3 due to emanation of the inner vessel of the radon monitor was observed. Using a steady gas flow through the radon monitor of 6 l/min, the gas will be replaced every 2 hours. Under these conditions the radon activity caused by emanation of the inner tank of the radon monitor should stay well below our detection limit of about 100-200 μBq.

In the last year, software based on Labwiew was developed and successfully tested. The software calculates the radon concentration based on the ^{214}Po and ^{218}Po peak intensity, the radon detector geometry as well as the calibration data.

11.3 Behavior of radon in liquid nitrogen and liquid argon

As it was shown recently (LNGS-EXP 33/05, add. 6/08, Appendix, par. 10.1.3), deposition of Rn daughters on the surface of stainless steel plates (SSP) in liquid nitrogen (LN_2) depends highly on the polarization and value of the applied voltage. The same results as for SSPs were obtained for Ge, Ge(Li) and Teflon plates, immersed both in LN_2 and in liquid argon.

We have investigated the Rn daughters deposition on SSPs placed inside a Faraday cage in LN_2. The experimental setup is shown on the left side of Figure 21. Several different voltages were applied to the cage and the SSP independently, including the same 2 kV potential on both. The latter case has shown one order of magnitude lower activity of Rn daughters collected on the SSP compared to the case of 2 kV applied to a SSP without the cage.

We have deduced the dependency of the Rn concentration growth in regions of LN_2 on time and on the HV connetcted to the SSPs. A new observation reveals the growth of the Rn concentration in time in a dewar itself, without placing any SSP. SSPs were immersed into the liquid nitrogen between long time periods only to perform measurements of the Rn concentration: A HV was applied for 3 hours to attract the Rn daughters to the surface of the SSPs for subsequent analysis in an alpha spectrometer. As a preliminary result, the Rn concentration growth in time in presence of SSPs on a high potential compared to the situation without any SSP yields no difference.

Presently, we perform measurements using a dewar with stainless steel inner container (V = 6.2 l) with Rn loaded LN_2 immersed in an outer dewar filled with LN_2 (see right side of Figure 21). The aim of this investigation is to eliminate an influence of convection. We are interested in the dependency of the Rn concentration growth in time on the flows in liquids. There is the suspicion that convection in LN_2 leads to the Rn concentration growth in a stream of a circulating liquid.

11.4 Gamma-ray screening

After the construction of the cryostat and the finalization of the design for the first detector strings the number of samples for gamma ray spectroscopy went down significantly. In the reporting period only four samples were measured: Dust, stainless steel cable chains, a coaxial cable and PEN foil. The dust sample was related to the question of the relatively high ^{222}Rn emanation rate of the cryostat. The U/Th/K activities lie in the same range as obtained in previous dust measurements. By comparing with the ^{222}Rn emanation data of the same sample (Table 1) one finds that ~ 12 % of the produced ^{222}Rn is emanated. The stainless steel cable chains will be used for the detector strings. Their activity is similar to what was measured before for stainless steel raw material except for ^{60}Co which is 10 times higher now. The difference might be attributed to few extra elements in the final cable chain with respect to the raw material. For the coaxial cable we found activites of U/Th in the range of 1 mBq/kg while the ^{40}K activity lies around 90 mBq/kg. Also we identified peaks for ^{108}Ag^m, ^{110}Ag^m and ^{7}Be (not shown in the table) corresponding to activities in

the mBq/kg range. Compared with a coaxial cable we tested earlier the present cable is more than 4 times cleaner in ^{40}K whereas the other isotopes show comparable activities. Finally, we found a very pure PEN foil (Teonex) which may be used for the production of radiopure flat cables. Previous measurements with ICP-MS indicated the potential purity of the PEN material, however, this is the first time that it could be confirmed by direct gamma ray screening. Further cross-checks with ICP-MS are planned for the near future.

Sample	Description	Emanation rate
Smaller micro switches	Type DG 13	(1.6 ± 0.6) μBq/piece
Larger micro switches	Type XCG5	(9.1 ± 1.7) μBq/piece
Black SIMRIT o-rings	15.9 mm x 2.6 mm	(34 ± 2) μBq/piece
Contact pins	Size 20 IMC	$<$ 0.4 μBq/piece
Differential pressure sensors	from BD-Sensors	(39 ± 6) μBq/piece
Thermovac pressure gauges	Type TR 100 (Leybold)	$<$ 6.3 μBq/piece
Dust	from LNGS (hall A)	(2.4 ± 0.2) Bq/kg
Black permanent marker	Type 280 (Schneider)	$<$ 0.45 mBq/m^2
Silvered screws	used for Cu-mounting	$<$ 2.2 μBq/piece
Cu bolts covered with cinder	used for Cu-mounting	(4.1 ± 0.5) mBq/m
Lint-free wipes	from KIMTECH	(5.7 ± 0.1) μBq/piece
Polyamide tube	10m, 8mm x 1mm	$<$ 7.1 μBq/m
Vacuum-insulated SS tube	10m, from DeMaCo	(24 ± 3) μBq/m
Flexible SS tube for vacuum	10m, 2 CF40 flanges	(4.8 ± 1.7) μBq/m
Flexible SS tube	15m, 1/2 inch	(32 ± 3) μBq/m
Single-serving Nitrile gloves	yellow, batch 1	(2.1 ± 0.2) mBq/piece
Single-serving Nitrile gloves	yellow, batch 2	(2.7 ± 0.1) mBq/piece
Multiple use Nitrile gloves	green, long sleeve	(75 ± 5) mBq/piece
Multiple use Viton gloves	black	(6.4 ± 1.3) mBq/piece
4-wire cable lake shore		$<$ 4.9 μBq/m
Multi-wire cable	from Buerklin	(63 ± 30) μBq/m
Abrasive paper	diamond, 9 micron	$<$ 15 μBq/g

Table 1: Measured ^{222}Rn emanation rates (saturation activities) for various samples.

Sample	specific activity [mBq/kg]				
	^{228}Th	^{238}U	^{226}Ra	^{40}K	^{60}Co
Dust from hall A	17600 ± 1500	—	19600 ± 1000	273000 ± 29000	$<$ 290
SS cable chains	2.2 ± 0.4	$<$ 72	1.0 ± 0.4	$<$ 3.1	190 ± 40
Coaxial cable	1.3 ± 0.4	$<$ 28	1.4 ± 0.4	90 ± 12	$<$ 0.37
PEN foil (Teonex)	$<$ 1.4	—	$<$ 2.0	$<$ 3.6	—

Table 2: Summary of gamma ray screening results.

References

[1] GERDA Status Report to the LNGS Scientific Committee (April 2008).

[2] NIER Ing., GERDA Risk Assessment Analysis Executive Summary (2006).

[3] M. Barnabé-Haider, S. Schönert, K. Gusev, GERDA Scientific / Technical Report GSTR-08-014

[4] Barbeau et. al., JCAP 0709:009, 2007

[5] Dr. Verplancke from Canberra Olen pointed out that standard BEGe detector should have similar field configurations and thus pulse shape properties as the detector used by Barbeau et. al., JCAP 0709:009, 2007.

[6] D. Zinato et al., *An alarm dispatcher system for Underground Physics Experiments*, submitted to IEEE Trans.Nucl.Sci..

[7] M. Bauer *et al.*, Journ. of Phys., Conf. Series **39** (2006) 362; Y.-D. Chan *et al.*, arXiv:0802.0860

[8] O.A. Ponkratenko *et al.*, Phys. Atom. Nucl. **63** (2000) 1282 and arXiv:nucl-ex/0104018.

[9] H.V. Klapdor-Kleingrothaus *et al.*, Phys. Lett. B **586** (2004) 198.

[10] L. Pandola *et al.*, Nucl. Instrum. Meth. A **570** (2007) 149.

[11] P. Peiffer, T. Pollmann, S. Schönert, A. Smolnikov and S. Vasiliev, JINST 3P08007 (2008).